A Neuron Enriched Nuclear Proteome Isolated from Human Brain

Eric B. Dammer[‡], **Duc M. Duong**[†], **Ian Diner**[†], **Marla Gearing**[⊥], **Yue Feng**[‡], **James J. Lah**[§], **Allan I. Levey**[§], and **Nicholas T. Seyfried**[†,§,*]

[‡]Department of Human Genetics

[†]Department of Biochemistry

[⊥]Department of Pathology and Laboratory Medicine

[‡]Department of Pharmacology

[§]Department of Neurology

Abstract

The brain consists of diverse cell types including neurons, astrocytes, oligodendrocytes and microglia. The isolation of nuclei from these distinct cell populations provides an opportunity to identify cell-type specific nuclear proteins, histone modifications and regulation networks that are altered with normal brain aging or neurodegenerative disease. In this study, we used a method by which intact neuronal and non-neuronal nuclei were purified from human post-mortem brain employing a modification of fluorescence activated cell sorting (FACS) we term fluorescence activated nuclei sorting (FANS). An antibody against NeuN, a neuron specific splicing factor, was used to isolate neuronal nuclei. Utilizing mass spectrometry (MS) based label-free quantitative proteomics we identified 1,755 proteins from sorted NeuN positive and negative nuclear extracts. Approximately 20 percent of these proteins were significantly enriched or depleted in neuronal versus non-neuronal populations. Immunoblots of primary cultured rat neuron, astrocyte and oligodendrocyte extracts confirmed that distinct members of the major nucleocytoplasmic structural linkage complex (LINC), nesprin-1 and nesprin-3, were differentially enriched in neurons and astrocytes, respectively. These comparative proteomic data sets also reveal a number of transcription and splicing factors that are selectively enriched in a cell-type specific manner in human brain.

Keywords

Cell type; astrocyte; neuron; oligodendrocyte; microglia; liquid chromatography coupled to tandem mass spectrometry (LC-MS/MS); transcription; splicing; nucleus; neuroproteomics; epigenetic

Introduction

Highly specialized cells including neurons, astrocytes, microglia, oligodendroglia, and vascular endothelial cells make up the architecture of the brain[1]. Each cell type has a unique gene expression profile and each is necessary for physiological function affecting behavior, learning, and memory[1, 2]. Due to alternative splicing and post translational modifications,

[*]Corresponding Author: Nicholas T. Seyfried, Departments of Biochemistry and Neurology, nseyfri@emory.edu, Emory University School of Medicine, Atlanta, Georgia 30322.

protein diversity dramatically exceeds RNA diversity[3], which argues for the direct evaluation of proteins in a cell-type specific manner. However, cellular heterogeneity in brain is often a direct hindrance towards this goal because proteins found in low abundance in neurons are often lost in a sea of proteins from more abundant glia. Therefore, methods that first isolate and purify homogeneous cell or even organelle populations from brain are necessary prior to mass spectrometry (MS) analysis to characterize cell-type specific proteomes. To this end, pioneering studies coupling fluorescence-assisted cell sorting (FACS)-based approaches[4, 5] have enabled RNA quantification from pure neurons and glia[6] isolated intact from mouse brain. Unfortunately these approaches would have limited value in post-mortem tissue since it is difficult to reproducibly isolate viable neurons and glia from these specimens. However, specific cellular organelles including nuclei are well preserved and can be isolated intact from postmortem brain[7, 8].

Nuclei are of particular interest because they contain transcription and splicing factors that regulate gene expression in a cell type specific manner[9]. The value of capturing a neuronal-specific nuclear proteome isolated from distinct brain regions is further underscored by the possibility of obtaining post-transcriptional and post-translational differences occurring with normal brain aging or disease. These differences in the proteome of neurons are likely to underlie key processes such as synaptic plasticity, learning and memory formation[10, 11]. Selective vulnerability of neurons is a common principle among neurodegenerative diseases, and in many of these diseases the pathological signatures often involve the loss, translocation, modification and/or aggregation of nuclear RNA or DNA binding proteins. Examples include the splicing factors TDP-43 and FUS in amyotrophic lateral sclerosis (ALS) and frontotemporal dementia (FTD)[12–15] and aberrant nuclear accumulation of cytoplasmic huntingtin in Huntington's Disease[16–18]. The way in which these nuclear proteins contribute to the disease pathophysiology remains a pressing question for researchers studying neurodegeneration at the molecular and cellular level. The gold standard for determining the relevance and applicability of any of the above protein changes occurring during normal brain physiological processes and neurodegeneration is to obtain direct proteomic identification and quantitation from well-defined nuclear subpopulations of distinct cell types from human brain.

In the current study, we used a method by which intact neuronal and non-neuronal nuclei were isolated from human postmortem brain employing a modification of fluorescence activated cell sorting (FACS) we term fluorescence activated nuclei sorting (FANS). Using a monoclonal antibody against the neuron specific splicing factor NeuN, we reproducibly isolated pure neuronal nuclear populations from human postmortem frontal cortex. NeuN is exclusively expressed in nuclei of most terminally differentiated neurons, with cerebellar Purkinje cells being a notable exception[19]. Liquid-chromatography coupled to tandem mass spectrometry (LC-MS/MS) was used to identify and quantify proteins across NeuN-positive and NeuN-negative nuclear populations. Approximately 20 percent of these proteins were significantly enriched or depleted in neuronal versus non-neuronal populations. These comparative proteomic data sets also reveal a number of transcription and splicing factors not previously known to be expressed in a cell-type specific manner in human brain. The methods described here will provide an unprecedented opportunity to identify cell-type specific nuclear proteins, histone modifications and regulation networks that may be altered in normal brain with aging or neurodegenerative disease.

Experimental Procedures

Initial nuclear isolation via sucrose density ultracentrifugation

Frozen, unfixed postmortem frontal cortex from four brains was obtained from the Emory University Brain Bank. Demographic information including age, gender and post-mortem

interval (PMI) for each case is provided Supplemental table 1. Preparation of nuclei was performed essentially as described[7, 8] with some modifications. Briefly, 1.0 to 1.5 g of thawed tissue was homogenized with 4 ml of lysis buffer [0.32 M sucrose, 5 mM $CaCl_2$, 3 mM $MgCl_2$, 0.1 mM EDTA, 10 mM Tris-HCl, pH 8.0, 0.1% v/v Triton X-100, 1× protease inhibitor cocktail (Roche), 5 mM iodoacetamide (Sigma), and 10 mM sodium butyrate (Sigma)] in a 7-mL capacity Dounce homogenizer for 40 strokes with pestle A (clearance: 76–127 μm) on ice. Homogenate was layered on top of a 14 × 89 mm polyallomer centrifuge tube (Beckman #331372) filled with 7 mL sucrose density cushion (1.8 M sucrose, 3 mM MgCl2 10 mM Tris-HCl, pH 8.0). Ultracentrifugation was performed at 36,000 rpm (222,000 rcf) for 120 min at 4°C in a Beckman Ti 41 swinging bucket rotor. Nuclear depleted supernatant above the cushion was removed and retained. Most of the sucrose cushion (approximately 7 mL) was aspirated without disturbing the nuclear pellet below. Phosphate buffered saline (PBS) plus inhibitors [protease inhibitor cocktail (Roche), 5 mM iodoacetamide (Sigma), and 10 mM sodium butyrate (Sigma)] was added to each tube and incubated on ice for 20 min to resuspend the pellet in low-viscosity conditions. Nuclei were triturated with a 1 mL capacity mechanical pipette for 30 to 60 s until clumps were visibly reduced. A small amount of nuclei was stained with Hoechst nuclear dye and examined under an Olympus BX51 microscope to visualize the extent of purity and intact status of the majority of nuclei. For estimating average nuclear diameter, 45 nuclei per group were imaged and then measured across two perpendicular axes to obtain an average individual diameter measurement. Bulk nuclei in PBS were collected in 1.5 mL microcentrifuge tubes (avoiding fast pipetting and using 1000 μL capacity pipette tips for transfer) and spun at 665 rcf on a tabletop centrifuge for 2 min at 4°C to obtain a loosely packed pellet of nuclei, typically in 30–60 μL. Nuclei recovery depends on several factors, including the amount of tissue homogenized, the homogenization efficiency (typically maintaining a higher proportion of intact nuclei with less force applied) and the brain region sampled.

Fluorescent staining of nuclei

Further preparation of fractionated nuclei for cytometry was performed essentially as described[7, 8] with attention given to the ratio of nuclei to fluorescent antibody conjugate required for successful sorting with high signal-to-noise. Estimated packed nuclear volume was used to adjust the volume of PBS used for resuspending each pellet (minimum resuspension volume, 500 μL). The excess volume(s) of resuspended nuclei were removed, combined and split into three aliquots used for calibrant staining as described below. Primary-secondary antibody conjugates were prepared in volume multiples of 50 μL PBS (per target nuclear pellet) with 25% blocking solution (0.5% BSA, 10% normal goat serum in PBS), with identical multiples of 1.5 μg primary antibody and 1.5 μg secondary antibody. Conjugate mixtures had a final primary antibody concentration of 30 μg/mL. The conjugates were allowed to assemble for 20 min in the dark at room temperature before addition of 50 μL of antibody conjugate to each nuclear pellet resuspension for a final volume of 550 μL. Typically two primary-secondary conjugate mixtures were made separately, one for mouse primary and one for rabbit primary, each conjugated with either Alexa Fluor® 488 (donkey anti mouse, Life Technologies) or phycoerythrin (PE; Jackson Immunoresearch)-labeled secondary antibodies, and added to each resuspended target nuclear pellet. In addition, 5 mM DRAQ5® DNA-binding dye (Cell Signaling) was added to resuspended nuclei-conjugate mixtures at 1:500 along with 0.08% v/v Triton X-100. The three aliquots of excess pooled nuclei, described above, were retained for single stained calibrants. Each aliquot was brought to 500 μL volume in PBS, with 0.08% v/v Triton X-100, and respectively exposed to i) DRAQ5® 1:500 alone; ii) DRAQ5® plus Alexa Fluor® 488-labeled antibody conjugate; or iii) DRAQ5® plus PE-labeled antibody conjugate. Additional controls which received only secondary antibodies were also prepared for determination of

background signal. Tubes were placed on their side on a rotating surface with 80 rotations per minute at 4°C in the dark for 5–8 h prior to cytometry.

Fluorescent activated nuclei sorting (FANS) and flow cytometry

FANS or flow cytometry was performed as described[7, 8] on a BD Biosciences FACSAria II or a BD Biosciences LSR II flow cytometer. Briefly, following calibration of the FACS machine or power-up of the flow cytometer, single-fluorophore stained nuclei or a mixture of single-stained nuclei with unstained nuclei were used as compensation controls to set automatic adjustments for overlapping fluorophore emissions between Alexa Fluor® 488 and PE in BD Biosciences FACSDiva software. Overlaps of the 488 and PE emission spectra with DRAQ5® far red emission were negligible. All nuclei were filtered into a 35 μm mesh-top polystyrene holding tube prior to sorting or cytometry. Initial sorting of nuclei for purity relied on gating of the events such that only DRAQ5®+/Histone H3(PE)+ singlet events representing nuclei were not sorted to waste. For sorting of neuronal and non-neuronal nuclei, gating of the nuclei was performed first upon the DRAQ5®/FSC (forward scatter, proportional to size) 2 dimensional plot, where single nuclei with at least 2N chromosomes (represented by the major DRAQ5® intensity peak) were selected. Subsequent gating was performed on the Alexa Fluor® 488/PE 2 dimensional plot. This allows selection of Alexa Fluor® 488/PE double-positive, double negative, or −/+ populations of nuclei. The populations sorted in this way included NeuN+/Histone H3+ and NeuN−/Histone H3+. Following FANS, each sample was tested for purity via an additional sort for up to 10,000 events using the same gating parameters so that population purity could be determined as a percentage of total second sort events. Additional flow cytometry was initially performed on secondary antibody only-stained control nuclei for comparison to Histone H3-PE antibody-conjugate stained nuclei, and on unlabeled nuclei for comparison to DRAQ5®-stained signal. FANS-sorted nuclei in sheath solution (PBS) were stored on ice immediately after collection. Samples were transferred to cold 15 ml Falcon tubes. For each 10 mL of sorted nuclei in PBS (sorting sheath solution), the following stabilizers were added: 2 ml of sucrose cushion, 200 μl 250 mM $CaCl_2$, and 200 μl 150 mM $MgCl_2$, plus inhibitors. Samples were capped and inverted 5 times before incubation on ice for 15 minutes. Visualization of intact nuclei via Alexa Fluor® 488 fluorescence was performed using 5–10 μl of post-sorted Alexa Fluor® 488+ nuclei. After incubation on ice, pellets of nuclei were obtained by spinning at 3,173 rpm (1,790 rcf) at 4°C in a swinging bucket rotor (Sorvall #75006445) for 15 minutes. Supernatant was removed and the nuclear pellet was dissolved in 50 μl 8M urea with 10 mM Tris-HCl pH 7.8 plus protease and phosphatase inhibitors (Halt, Thermo Pierce Corporation). DNA was sheared by 5 cycles of 1 s sonication with a microtip sonicator at 20 percent power followed by at least a 10 s rest on ice. Protein concentration for each sample was determined by bicinchoninic acid (BCA) assay.

Peptide identification and quantification

Equal protein amount (determined by BCA) of total homogenate, soluble, pre-FANS, and post-FANS nuclear samples were digested in solution according to the established protocol for reduction, alkylation, and LysC plus trypsin digestion[20]. An equal volume of each peptide sample resuspended in loading buffer (0.1% formic acid, 0.03% trifluoroacetic acid, 1% acetonitrile) was loaded onto a 21 cm nano-HPLC column (internal diameter 100 μm) packed with Reprosil-Pur 120 C18-AQ 1.9 μm beads (Dr. Maisch) and eluted over a 2 h 4– 80% buffer B reverse phase gradient (Buffer A: 0.1% formic acid, 1% acetonitrile in water; Buffer B: 0.1% formic acid in acetonitrile) generated by a NanoAcquity UPLC system (Waters Corporation). Peptides were ionized with 2.0 kV electrospray ionization voltage from a nano-ESI source (Thermo) on a hybrid LTQ XL Orbitrap mass spectrometer (Thermo). Data dependent acquisition of centroid MS spectra at 30,000 resolution and MS/

MS spectra were obtained in the LTQ following collision induced dissociation (collision energy 35%, activation Q 0.25, activation time 30 ms) for the top 10 precursor ions with charge determined by the acquisition software to be z 2. Higher energy collisional dissociation (HCD) was not used and the "exclude isotope peak" setting was on. Dynamic exclusion of peaks already sequenced was for 20 s with early expiration for 2 count events with signal-to-noise > 2. Automatic gating control was set to 150 ms maximum injection time or 10^6 counts. For each post-sorted biological replicate, a second 2 h round of loading, elution, and data dependent acquisition was performed with all previously sequenced peaks excluded from analysis, to increase depth of coverage and the variety of peptides sequenced, providing higher spectral counts from unique peptides for each identified protein, and increasing protein identifications. The SageN Sorcerer SEQUEST 3.5 algorithm was used to search and match MS/MS spectra to a complete semi-tryptic human proteome database (NCBI reference sequence revision 50, with 66,652 entries) plus pseudo-reversed decoys sequences[21, 22] with a 20 ppm mass accuracy threshold. Only b and y ions were considered for scoring (Xcorr) and Xcorr along with ΔCn were dynamically increased for groups of peptides organized by a combination of trypticity (fully or partial) and precursor ion charge state to remove false positive hits along with decoys until achieving a false discovery rate (FDR) of < 5% (< 0.25% for proteins identified by more than one peptide). The FDR was estimated by the number of decoy matches (nd) and total number of assigned matches (nt). FDR = 2*nd/nt, assuming mismatches in the original database were the same as in the decoy database[23]. To remove redundancy, proteins that shared peptides were clustered into a single group and represented by the one protein with the highest number of spectral counts. Peptide/protein quantification was performed based on the extracted ion current (XIC) measurements of identified peptides. Peptide-specific ion current intensities were extracted and compared across cases using in-house software (DQuan) as previously described[24, 25]. Accurate peptide mass and retention time was used to derive signal intensity for every peptide across LC-MS/MS runs for each case. For those proteins identified by 3 peptides we averaged the extracted ion intensities for the three most intense tryptic peptides to derive a relative protein abundance measurement for each identified protein. The same exact three peptides for each protein were used to derive an average signal-to-noise ratio for each protein across runs which has been determined to correspond with an accurate, low-variance measurement of a protein's abundance[26]. Protein quantification was performed across eight total LC-MS/MS runs from four NeuN positive and four NeuN negative samples (four biological replicates). Student's T-test ($p < 0.05$), was used to compare protein abundances, thereby strictly identifying proteins as neuronal and non-neuronal enriched. For comparison, the average coefficient of variance for proteins identified and quantified as significantly enriched or depleted from NeuN positive nuclei by 2 unique peptides was 37 ± 12%, whereas all other proteins were quantified by 3 unique peptides with an average variance of 30 ± 13%. Proteins that were significantly depleted or enriched, but quantified by a single peptide, were not considered in the final analysis. These measures for biological variance are in accord with previously published measures of another study, which analyzed cell-line derived label free quantified proteins[27].

Bioinformatics: cellular compartment enrichment/depletion analysis

For determination of the effect of nuclear purification in depleting or enriching proteins from the various cellular compartments, total homogenate, pre-sorted nuclei, and post-FANS nuclei (DRAQ5®+/histone H3+) were comparatively analyzed by LC-MS/MS. Following DQuan quantitation, three protein abundance comparisons were made: i) between pre-sorted nuclei and total homogenate; ii) between post-FANS nuclei and total homogenate; and iii) between post-FANS nuclei and pre-sorted nuclei. Proteins with more than 20 percent enrichment in the first two comparisons or more than 20 percent enrichment in the first and 10 percent enrichment in the third comparison were considered as a preliminary pool of

proteins that may harbor enriched groups of proteins. Proteins with more than 20 percent depletion in the first two comparisons or more than 40 percent depletion in the third comparison were considered as a preliminary pool of proteins potentially harboring groups of depleted proteins. To identify these groups, gene symbols for the preliminary lists of depleted or enriched proteins were submitted for DAVID ontology analysis[28] and sublists of significantly overrepresented groups of proteins from various cellular components were generated. Average abundance ratios representing an estimate of the overall change in protein abundance from each compartment were calculated. Only compartments appearing in one, but not both (e.g. ribosomes), of the lists were considered—with the exception of proteasome subunits, because there was a perfect subdivision of the category, indicating that only core 20S α and β subunits were depleted and only 19S cap subunits were enriched. Cutoffs for DAVID analysis of 10 or 20 percent were allowed (even though variance was determined to be on average 30 percent—see above methods section) because DAVID only supplies enriched protein sublists back for cellular compartments if they are related and overrepresented, regardless of stringency, and the averages for protein sublists would be skewed away from zero if the compartment specific sublists were not allowed to be as inclusive as possible.

Bioinformatics: clustering analysis

Clustering to obtain the dendrogram of sample relatedness between the eight post-FANS quantified proteomes was performed in Broad Institute's GenePattern 3.4[29]. Hierarchical Clustering 5.0 and Hierarchical Clustering Viewer 9.0 modules were generated using open source libraries[30] inputting the list of $\log_2$ transformed abundances for protein homology group leaders. City block distance metric was used. Abundance Z-scores were generated for each data point by normalizing protein abundances to the geometric mean for each individual protein across samples (n=8) and $\log_2$ transformed before being used to generate a heat map (Cytoscape 2.8.2)[31] representing sample-to-sample differences between neuronal or non-neuronal nuclei enriched proteins using ClusterMaker 1.9 plugin for Cytoscape which performed 1000 iterations of k-means clustering (n=5 clusters). Output was exported as a .cdt file and the top two largest clusters which happened to represent neuronal nuclei-enriched (487 proteins) and non-neuronal nuclei-enriched (420 proteins) were visualized using Java TreeView 1.1.6r2.

Bioinformatics: neuronal nuclei interactome/connectivity analysis

Significantly enriched proteins in neuronal nuclei as determined by t-test comparison of abundances in neuronal and non-neuronal nuclei quantified proteomes were assembled into a gene symbol list, which was used as input for STRING 9.0[32, 33]. Allowed interactions were required to score better than a 0.25 (from 0 to 1), and only known interactions from experimental evidence and/or in curated interaction databases were allowed. K-means clustering (n=12 clusters) was performed and the interactive graphical visualization was manually organized to provide a view of the clusters as well as cluster-to-cluster connectivity.

Western blotting and primary cell culture

Western blotting was performed on Millipore Immobilon PVDF membrane following overnight wet transfer and 1–2 h of blocking in Tris buffered saline plus 5% (wt/vol) bovine serum albumin as previously described[20]. Most antibodies and stains used in this study were obtained from Abcam with the following exceptions: Anti-NeuN mouse monoclonal were from Chemicon (Millipore), a rabbit polyclonal anti-QKI-5 from Bethyl Laboratories, anti-PTBP2 from Novus, anti-TDP43 from ProteinTech and anti-GFAP from Biocare Medical. Rat brain primary neurons, astrocytes, and oligodendroglia were isolated from embryonic or

neonatal Sprague-Dawley rats as previously described[23]. Cultured cells were washed in PBS and harvested in Laemmli buffer prior to SDS-PAGE and western blotting.

Results

Proteomic analysis of nuclei from human brain

A workflow was adapted to obtain intact nuclei from postmortem human brain tissue via ultracentrifugation following tissue homogenization in which supernatant (**S**) and nuclei (**N**) fractions were obtained from total homogenate (**H**) (Figure 1A). For sorting of nuclei by FANS, intact nuclei (**N**) were stained with the DNA-intercalating, fluorescent dye DRAQ5® and a fluorescent conjugate of an antibody to histone H3 and purified (**P**) to homogeneity (Figure 1C), as discussed in detail below. After the first purification step the homogenate, supernatant and nuclear fractions showed significant differences in protein composition by Coomassie blue staining following gel electrophoresis (Figure 1B). Lower molecular weight (MW) histones (approximately 12–15 kDa) were enriched in nuclear extracts, compared to the supernatant and total homogenates. To further characterize the extent of nuclear enrichment by centrifugation, we performed quantitative LC-MS/MS of equal amounts of trypsin-digested protein from homogenate, supernatant and nuclear fractions (Figure 1A, dashed arrows). Among the proteins identified, we selected ATP synthase δ, rho GDP dissociation inhibitor (GDI) α, and hnRNP A0, as mitochondrial, cytoplasmic, and nuclear markers, respectively, based on their established functional roles. A representative, extracted ion chromatogram (XIC) for a unique tryptic peptide representing each of the above marker proteins across the **H, S**, and **N** fractions is provided (Figure 2A–C). Comparisons of relative abundance of the selected ATP synthase peptide indicated that this mitochondrial protein was depleted from both **S** and **N** fractions, but present in the starting material, **H** (Figure 2A). A rho GDI α peptide was enriched in **S** relative to **H** and undetectable in **N** (Figure 2B). The nuclear marker hnRNP A0 peptide was enriched approximately 20-fold in **N** relative to **H** and undetectable in **S** (Figure 2C). To further confirm these results, we blotted biological replicates of the same three fractions for rho GDI α and hnRNP A0 (Figure 2D) and obtained results which paralleled the XIC based quantification, although the dynamic range of the blot was not sufficient to permit detection of hnRNP A0 in **H**. These observations support the conclusion that the nuclear isolation procedure effectively separates intact nuclei from mitochondrial and cytoplasmic components in postmortem human brain.

Negligible postmortem effects on brain nuclear integrity and protein stability

In order to perform FANS, intact nuclei must first be recovered from homogenized tissue. Confirming nuclear integrity insures that the proteome obtained from sorted nuclei represents intact, rather than fragmented nuclei which may systematically lack some components. Therefore, nuclei were examined both microscopically and biochemically for effects of postmortem interval (PMI) over a range of PMI from 5 h to 28 h. The vast majority of nuclei recovered appeared intact by visual inspection of Hoechst stained material (Figure 3A–D), with an average diameter of 7 μm, and which did not significantly change with increasing PMI (Figure 3E). Protein banding visualized via SDS-PAGE of nuclear extracts from the same cases further supported the conclusion that the proteome was not compromised, grossly altered, nor degraded comparing PMIs of 5 h to as long as 28 h (Figure 3F). A more stringent test of the integrity of the proteome involves observing the extent of *in vivo* protease degradation by measuring partial-tryptic protein cleavage events at the peptide level by mass spectrometry[34]. LC-MS/MS analysis and database searching of four human nuclear extracts lysed before or after FANS indicated that approximately 2–4% of total spectral counts matched partial tryptic peptides across all cases. Notably, PMI had no effect on this average, as determined by a nearly flat trendline slope (Figure 3G). These results are in line with previous reports that brain nuclei are resistant to postmortem

degradation or structural changes, in comparison to nuclei of other tissues and cytoplasmic proteins within brain[35, 36]. Moreover, one study also found no significant effect of frozen storage time on nuclear immunoreactivity for FANS analysis[35].

FANS further improves the purification of nuclei

LC-MS/MS identifications from intact nuclei after centrifugation (fraction **N**) included non-nuclear proteins typically associated with extracellular matrix (ECM) including laminin, fibrillin, tenascin, collagen and agrin. To assess whether the FANS isolation improved purity, intact nuclei were stained with DRAQ5® and a fluorescent conjugate of histone H3 antibody, as described above. Sorting with these markers provided excellent fluorescent signal to noise ratio (Supplemental Figure 1). Positive events in the whole population of stained nuclei consistently indicated a purity of unsorted nuclei **N** above 90 percent for all sorted events (Supplemental Figure 1A, B). Quantification of all protein markers of various cellular compartments was performed as described in methods and is summarized in Figure 4, while all individual quantifications are provided in Supplemental Table 2. Protein quantifications indicated that each of the above mentioned ECM proteins was detected as more than four-fold increased in fraction **N**. Average protein abundance for all annotated ECM proteins was 846 ±156% the level detected in **H** (Figure 4). However, comparative analysis of the post-FANS sorted nuclei (**P**) reveals that ECM components could still be separated from nuclei (depleted 96 percent in fraction **P** relative to fraction **N**, to nearly half of the average signal for ECM proteins in **H**. We also noted that protein abundances from all non-nuclear cellular components were further depleted in fraction **P** compared to **N**, with the population average falling from greater than one-half the level seen in **H** to less than one-quarter the level in **H**. We conclude from these data that FANS further purifies nuclei from non-nuclear contaminants. Notably, two protein groups in Figure 4 showed a distinct trend. First, co-enrichment of endoplasmic reticulum proteins with fraction **N** was partially lost in fraction **P**, suggesting that endoplasmic reticulum, although continuous with the nuclear envelope, is nonetheless delicate and probably stripped away in part through the FANS process. Second, proteasome subunits segregated as two distinct groups, with 19S cap subunits enriched within brain nuclei. However, 20S alpha and beta core subunits, which bear the catalytic sites required for proteolysis by the proteasome, were largely absent in FANS purified nuclei (**P**) or by centrifugation alone (**N**). This finding is consistent with 19S regulatory particle functions in the nucleus that may be independent of proteasome core catalytic activity[37].

The above comparative analysis was conducted on equally loaded peptide amounts from centrifugation-purified, **N**, and further, FANS-purified, **P**, nuclei as well as total frontal cortex homogenate, **H**. However, while centrifugation typically recovered over 2 percent of **H** protein weight (1.5 mg **N** from 70 mg of **H**, recovered from 1.0 g of frontal cortex), considerably less protein yield (1% or lower) was achieved in **P** after further FANS purification of nuclei. This is consistent with the consideration that the FANS purification protocol necessarily employs a small amount of Triton X-100 during homogenization to effectively release nuclei from cells, and permeabilization before FANS with additional Triton X-100 allows antibody conjugates access to the intranuclear compartment. Thus, the protocol also probably allows freely diffusible nuclear proteins to be lost. This is consistent with a somewhat lower protein yield after FANS than expected based on the known average weight of protein per nucleus from mammalian brain (~100 pg)[38]. Typically, **P** recovered protein from 5 million nuclei (counted by FANS) starting from 1.0 g of tissue, whereas the above weight of **N** would have us estimate a possible yield of 15 million. Thus, while a good deal of protein lost post-FANS is likely due to the removal of non-nuclear impurities, if all nuclear contents need to be preserved during FANS, other protocols which do not require envelope permeabilization should be used[39]. However, short of using an antibody against

cell-type specific antigen(s) displayed on the nuclear envelope, where no such antigens are yet established, there is no other available technique for isolation of human postmortem nuclei subpopulations.

FANS isolates neuronal specific nuclei

Having established a method that efficiently purifies nuclei from frontal cortex, we set out to isolate and quantify the proteome of neuronal nuclei and non-neuronal nuclei from the same region of human brain. A mouse monoclonal antibody against NeuN, the neuron specific splicing factor and RBFOX3 gene product[40, 41], was used to stain isolated nuclei for FANS. As in the above described workflow, separation of nuclei from non-nuclear contaminants relied upon a positive signal for both DNA and histone H3. In addition, sorting of nuclei was dependent upon NeuN staining intensity, with NeuN positive and negative nuclei showing spatial separation (Figure 5, *left panel*). To check purity of the two populations, after initial sorting, some of the nuclei from each were subjected to a second sort (capturing 10,000 events). This demonstrated that greater than 99 percent of NeuN negative nuclei were retained in the Alexa Fluor® 488-PE intensity plot whereas NeuN positive nuclei consistently gated more than 90 percent (Figure 5, *middle and right panel*). Similar results were obtained across all four biological replicates in this study. As expected, intact NeuN positive nuclei were the vast majority of the visible objects in fluorescent microscopy performed on NeuN sorted nuclei (Figure 5, *right panel inset at top left*). Quantitative proteomics was performed on equal amounts of trypsin-digested protein from each of the four resulting NeuN-positive and NeuN-negative samples. Average abundance for the 1,755 quantified proteins (provided with quantitation in Supplemental Table 3) was normalized to the mean of the eight measurements and all proteins were grouped into k means clusters that had a similar expression profile across the eight samples as described in experimental procedures. The top two largest clusters represent 487 NeuN positive nuclei-enriched proteins, and 420 NeuN negative nuclei-enriched proteins (Figure 6A). Unsupervised hierarchical clustering was also able to correctly distinguish and gauge the relatedness of the two groups of samples (Figure 6A, *dendrogram at top*). Gene symbols for proteins with a particularly stark contrast between the two nuclear populations are provided to the right of the heat map. Strikingly, 14 proteasome regulatory particle 19S cap subunits were identified in this manner as neuronal nuclei enriched, consistent with the finding presented earlier that 19S cap regulatory subunits are enriched in frontal cortex nuclei, but further restricting the source of this enrichment to neuronal nuclei. A more statistically rigorous approach (Student's T-test, $p<0.05$) was used to compare protein abundances across the four NeuN-positive and -negative samples, thereby strictly identifying 182 proteins as neuronal nuclei enriched (*complete list with p values provided in* Supplemental Table 4) and 166 proteins as non-neuronal nuclei enriched (Supplemental Table 5). Thus, approximately 20 percent of these proteins were significantly enriched or depleted in neuronal versus non-neuronal populations. Representative neuron-enriched proteins from the complete list in Supplemental Table 4 are also provided in Table 1.

Sampling variability can increase variance between samples, which decreases sensitivity of the T-test to obtain significantly enriched proteins listed in Supplemental Tables 4 and 5. Therefore, we also performed a T-test ($p<0.05$) to find proteins for which the four calculated ratios for biological replicates (NeuN positive/negative abundance) are significantly different from their inverse values, thereby rescuing 12 neuronal nuclei enrichment identifications and 17 non-neuronal nuclei enriched proteins (Supplemental Table 6). Overall, the identification of proteins involved in neuronal functions enriched in NeuN-positive nuclei, including NeuN/RBFOX3 itself, calcium/calmodulin-dependent kinases, and neuronal polypyrimidine tract binding protein (PTBP2) confirmed the efficiency of sorting (Figure 6A and Supplemental Tables 4 and 6). In addition, the enrichment of

oligodendroglia-resident 2',3' cyclic nucleotide phosphodiesterase (CNP), and the splicing factor quaking (QKI), was confirmed in the NeuN-negative population (Figure 6A and Supplemental Table 5).

To assess the cell-type specificity of novel enriched proteins, cultured primary rat brain cells were isolated and purified to homogeneous populations of neurons, astrocytes, or oligodendroglia. The relative purity of these populations was demonstrated by Western blotting for established markers of neurons (NeuN, and neuronal PTB), astrocytes (GFAP), and oligodendroglia (CNP, and QKI) as shown in Figure 6B. Interestingly, the two paralogs nesprin-1 (SYNE1) and nesprin-3 (SYNE3) appeared in the above quantitative analysis to be neuronal and non-neuronal nuclear enriched, respectively (Figure 6A). Indeed, western blotting for these proteins in the three primary cell populations confirmed that nesprin-1 is preferentially enriched in primary neurons, whereas nesprin-3 is robustly enriched predominantly in astrocytes (Figure 6B). We further demonstrated nesprin-1 positive neuronal nuclear staining, which co-segregated with the fluorescent signal for NeuN positive nuclei by flow cytometry (Figure 6C). Nesprins are proteins which harbor a transmembrane domain to cross the outer leaflet of the nuclear envelope. They also contain a hydrophobic linker that crosses perinuclear space to form a complex using spectrin repeats that avidly interact with the cytoplasmic cytoskeleton, microtubules, and/or intermediate filaments. To bridge these protein interactions to the nuclear lamina inside the nuclear envelope, nesprins utilize a unique domain at their C-terminus that interacts specifically with SUN domain proteins in the inner leaflet of the nuclear envelope[42]. Thus, the complex is called linker of nucleoskeleton and cytoskeleton (LINC). In so doing, nesprins are implicated in nuclear positioning and local cytoskeletal organization, and provide a means for forces to be transmitted to the nucleus for its participation in cellular migration[43]. Further supporting differences in LINC architecture between neurons and other cell types, we also found a significant depletion of SUN2 in neurons (>8 fold enriched in the non-neuronal population, p<0.05; Supplemental Table 5). Finally, the software STRING 9.0 was used to interrogate the extent of protein-protein interactions and their implied functions in the neuronal and non-neuronal nuclear enriched protein populations (Supplemental Figure 2). Neuronal proteins were much more likely to interact with one another (>2.6 interactions per protein, maximum 500 interactions reached) than non-neuronal nuclear proteins (<1.2 interactions per protein). The network of neuronal nuclear proteins is shown in Supplemental Figure 2, with the 19S regulatory proteasome cap components prominently connected to other clusters of the network that contain core splicing factors and general transcription factors.

Discussion

In this study, we took advantage of the previously described greater ability of nuclei than cells to survive in post-mortem tissue[35, 36] to allow reproducible fractionation and enrichment suitable for proteome analyses. We developed a method to effectively separate intact neuronal and non-neuronal nuclei from human postmortem brain, employing FANS. This approach not only significantly increases the purity of nuclei, but also provides a platform by which cell type specific nuclear subpopulations can be isolated from brain. In particular, FANS coupled to LC-MS/MS performed on neuronal and non-neuronal nuclear protein extracts revealed that approximately 20 percent of the 1,755 identified proteins were significantly enriched or depleted in neuronal versus non-neuronal populations. Among these, 19S proteasome regulatory subunits and nesprin-1 were enriched in neuronal nuclei. Conversely, nesprin-3 was significantly enriched in non-neuronal nuclei. Therefore, separating nuclear subpopulations for quantitative proteomics has revealed a greater level of complexity in brain organization than may have been previously appreciated.

Our first notable finding was the restriction of the 19S proteasome regulatory particle subunits to neuronal nuclei, along with co-enrichment of a subset of core transcription machinery discussed here. 19S association with gene promoters and stimulation of transcription occurs through either the SAGA histone acetyltransferase complex[44, 45], or the more general transcription factor complex TFIID that engages promoters concomitant with TATA-binding protein recruitment[46]. Both complexes are conserved from yeast to humans and recruitment of either activation complex precedes chromatin modifications which coincide with RNA polymerase II access and transcription from inducible genes. Interestingly, two TATA-binding protein associated factors TAF15 and BTAF1 ATPase were also expressed at significantly higher levels in neuronal nuclei. Moreover, a subunit of TFIIH was also found enriched in neuronal nuclei (GTF2H1 in Supplemental Table 4). The core transcription complexes of which these factors are members have been demonstrated to enforce a high transcription rate in an ATP-dependent fashion by promoting re-initiation of the transcription cycle[47]. This may suggest that neurons support robust transcription rates via deployment of these factors to promoters of induced genes. A role for 19S ATPase activity in this process remains to be tested. Also consistent with a higher capacity for transcriptional throughput of neurons, we found that RNA maturation machinery, i.e. cleavage and polyadenylation specific factors (CPSF) 1, 2, and 6 were enriched in neurons (Supplemental Table 4). Given this abundance of CPSF in neurons, we speculate a potential downside is that the pre-mRNA of neurons may have a higher propensity to undergo premature cleavage and polyadenylation than pre-mRNA of other, non-neuronal cell types[48, 49]. A second major finding was the cell-type specific enrichment of nesprin paralogs 1 and 3 to nuclei of neurons and astrocytes, respectively. In addition to their roles in linking nuclear cytoskeleton to cytoplasmic structural elements, ChIP experiments suggest that nesprins may also anchor centromeric chromatin and other heterochromatin to the nuclear envelope in an alternate orientation[50]. Thus, our findings suggest that LINC structure-function affecting heterochromatin maintenance and possibly mechanotransduction of signals to the nucleus are distinct in neurons and astrocytes, a hypothesis that requires further testing.

The finding that proteins enriched in neuronal nuclei have a much greater propensity to interact in functional complexes than proteins enriched in non-neuronal nuclei is consistent with the knowledge that neuron-specific proteins are derived from a more homogeneous population, as opposed to multiple cell types with independent interactomes. Purification of a homogeneous population of fluorescently tagged nuclei in animal models has also demonstrated six-fold increased sensitivity for cell-type specific identification of down-regulated genes[51]. These data highlight the benefit of deeper biological insight made possible by selecting specific markers for sorting that result in enriched cell-specific nuclear populations for downstream applications. In the future, we envision that the methods used here will be used to separate nuclei from different brain regions, conditions, and cell-types, and even neuronal sub-types unique to different cortical layers[52]. This approach will also empower research discoveries on nuclear changes occurring during disease progression, especially in rare but important populations, such as immune cell types present in the brain, which are thought to be critical in neuroprotective and neuroinflammatory processes[53]. For example, activated microglia might be selected from nuclei stained with microglial marker Iba1 and nuclear-translocated NFkB, a pro-inflammatory transcription factor that is excluded from the nucleus in the absence of activating stimuli[54].

Some of the above approaches will likely be useful in elucidating the biological significance of findings in the current study. Purified subpopulations of nuclei from tissue are suitable for multiple downstream applications in complementary analyses. A few examples include RNA-Seq and ChIP-Seq for transcriptomics, epigenetics, or splicing assays to determine cell-type specific differences in RNA processing. Another possibility is to extract histones

for cell-type specific global profiling of post translational modifications[55]. For example, differences in histone acetylation have been measured in Alzheimer's Disease (AD) nuclear extracts isolated from human brain[56]. Whether cell-specific subpopulations are more vulnerable to these histone alterations in AD brain is unclear. Use of FANS would allow quantification of neuronal specific histone acetylation in AD brain that could be used to gauge efficacy of therapeutic histone deacetylase (HDAC) inhibitors in a cell type-specific manner.

In conclusion, the respective differences between neuronal and non-neuronal nuclei are consistent with neuronal specific transcription program(s) and adaptations of neuronal and astrocyte LINC structure-function. Given that the method performed here is scalable and may be adaptable to virtually any tissue, and any cell-type for which FANS-compatible marker staining is possible, we foresee this approach being widely applied to obtain nuclei suitable for a number of downstream applications which provide information complementary to quantitative proteomics.

Supplementary Material

Refer to Web version on PubMed Central for supplementary material.

Acknowledgments

References

1. Lyck L, Dalmau I, Chemnitz J, Finsen B, Schrøder HD. Immunohistochemical Markers for Quantitative Studies of Neurons and Glia in Human Neocortex. Journal of Histochemistry & Cytochemistry. 2008; 56(3):201–221. [PubMed: 17998570]

2. Fields RD, Stevens-Graham B. New Insights into Neuron-Glia Communication. Science. 2002; 298(5593):556–562. [PubMed: 12386325]

3. Kelleher N. A Cell-Based Approach to the Human Proteome Project. Journal of The American Society for Mass Spectrometry. 2012; 23(10):1617–1624. [PubMed: 22976808]

4. Lobo MK, Karsten SL, Gray M, Geschwind DH, Yang XW. FACS-array profiling of striatal projection neuron subtypes in juvenile and adult mouse brains. Nat Neurosci. 2006; 9(3):443–452. [PubMed: 16491081]

5. Sugino K, Hempel CM, Miller MN, Hattox AM, Shapiro P, Wu C, Huang ZJ, Nelson SB. Molecular taxonomy of major neuronal classes in the adult mouse forebrain. Nat Neurosci. 2006; 9(1):99–107. [PubMed: 16369481]

6. Cahoy JD, Emery B, Kaushal A, Foo LC, Zamanian JL, Christopherson KS, Xing Y, Lubischer JL, Krieg PA, Krupenko SA, Thompson WJ, Barres BA. A Transcriptome Database for Astrocytes, Neurons, and Oligodendrocytes: A New Resource for Understanding Brain Development and Function. The Journal of Neuroscience. 2008; 28(1):264–278. [PubMed: 18171944]

7. Jiang Y, Matevossian A, Huang H-S, Straubhaar J, Akbarian S. Isolation of neuronal chromatin from brain tissue. BMC Neuroscience. 2008; 9(1):42. [PubMed: 18442397]

8. Matevossian A, Akbarian S. Neuronal Nuclei Isolation from Human Postmortem Brain Tissue. J Vis Exp. 2008; (20):e914.

9. Ma Y-C, Song M-R, Park JP, Henry Ho H-Y, Hu L, Kurtev MV, Zieg J, Ma Q, Pfaff SL, Greenberg ME. Regulation of Motor Neuron Specification by Phosphorylation of Neurogenin 2. Neuron. 2008; 58(1):65–77. [PubMed: 18400164]

10. Lai K-O, Zhao Y, Ch'ng TH, Martin KC. Importin-mediated retrograde transport of CREB2 from distal processes to the nucleus in neurons. Proceedings of the National Academy of Sciences. 2008; 105(44):17175–17180.

11. Lee S-H, Lim C-S, Park H, Lee J-A, Han J-H, Kim H, Cheang Y-H, Lee S-H, Lee Y-S, Ko H-G, Jang D-H, Kim H, Miniaci MC, Bartsch D, Kim E, Bailey CH, Kandel ER, Kaang B-K. Nuclear Translocation of CAM-Associated Protein Activates Transcription for Long-Term Facilitation in Aplysia. Cell. 2007; 129(4):801–812. [PubMed: 17512412]

12. Dammer EB, Fallini C, Gozal YM, Duong DM, Rossoll W, Xu P, Lah JJ, Levey AI, Peng J, Bassell GJ, Seyfried NT. Coaggregation of RNA-Binding Proteins in a Model of TDP-43 Proteinopathy with Selective RGG Motif Methylation and a Role for RRM1 Ubiquitination. PLoS ONE. 2012; 7(6):e38658. [PubMed: 22761693]

13. King OD, Gitler AD, Shorter J. The tip of the iceberg: RNA-binding proteins with prion-like domains in neurodegenerative disease. Brain Research. 2012; 1462(0):61–80. [PubMed: 22445064]

14. Kwiatkowski TJ, Bosco DA, LeClerc AL, Tamrazian E, Vanderburg CR, Russ C, Davis A, Gilchrist J, Kasarskis EJ, Munsat T, Valdmanis P, Rouleau GA, Hosler BA, Cortelli P, de Jong PJ, Yoshinaga Y, Haines JL, Pericak-Vance MA, Yan J, Ticozzi N, Siddique T, McKenna-Yasek D, Sapp PC, Horvitz HR, Landers JE, Brown RH. Mutations in the FUS/TLS Gene on Chromosome 16 Cause Familial Amyotrophic Lateral Sclerosis. Science. 2009; 323(5918):1205–1208. [PubMed: 19251627]

15. Neumann M, Sampathu DM, Kwong LK, Truax AC, Micsenyi MC, Chou TT, Bruce J, Schuck T, Grossman M, Clark CM, McCluskey LF, Miller BL, Masliah E, Mackenzie IR, Feldman H, Feiden W, Kretzschmar HA, Trojanowski JQ, Lee VM-Y. Ubiquitinated TDP-43 in Frontotemporal Lobar Degeneration and Amyotrophic Lateral Sclerosis. Science. 2006; 314(5796):130–133. [PubMed: 17023659]

16. Saudou F, Finkbeiner S, Devys D, Greenberg ME. Huntingtin Acts in the Nucleus to Induce Apoptosis but Death Does Not Correlate with the Formation of Intranuclear Inclusions. Cell. 1998; 95(1):55–66. [PubMed: 9778247]

17. Schilling G, Becher MW, Sharp AH, Jinnah HA, Duan K, Kotzuk JA, Slunt HH, Ratovitski T, Cooper JK, Jenkins NA, Copeland NG, Price DL, Ross CA, Borchelt DR. Intranuclear Inclusions and Neuritic Aggregates in Transgenic Mice Expressing a Mutant N-Terminal Fragment of Huntingtin. Human Molecular Genetics. 1999; 8(3):397–407. [PubMed: 9949199]

18. Sieradzan KA, Mechan AO, Jones L, Wanker EE, Nukina N, Mann DMA. Huntington's Disease Intranuclear Inclusions Contain Truncated, Ubiquitinated Huntingtin Protein. Experimental Neurology. 1999; 156(1):92–99. [PubMed: 10192780]

19. Mullen RJ, Buck CR, Smith AM. NeuN, a neuronal specific nuclear protein in vertebrates. Development. 1992; 116(1):201–211. [PubMed: 1483388]

20. Herskowitz JH, Seyfried NT, Duong DM, Xia Q, Rees HD, Gearing M, Peng J, Lah JJ, Levey AI. Phosphoproteomic Analysis Reveals Site-Specific Changes in GFAP and NDRG2 Phosphorylation in Frontotemporal Lobar Degeneration. Journal of Proteome Research. 2010; 9(12):6368–6379. [PubMed: 20886841]

21. Elias JE, Gygi SP. Target-decoy search strategy for increased confidence in large-scale protein identifications by mass spectrometry. Nat Meth. 2007; 4(3):207–214.

22. Xu P, Duong DM, Peng J. Systematical Optimization of Reverse-Phase Chromatography for Shotgun Proteomics. Journal of Proteome Research. 2009; 8(8):3944–3950. [PubMed: 19566079]

23. Seyfried NT, Gozal YM, Donovan LE, Herskowitz JH, Dammer EB, Xia Q, Ku L, Chang J, Duong DM, Rees HD, Cooper DS, Glass JD, Gearing M, Tansey MG, Lah JJ, Feng Y, Levey AI, Peng J. Quantitative Analysis of the Detergent-Insoluble Brain Proteome in Frontotemporal Lobar Degeneration Using SILAC Internal Standards. Journal of Proteome Research. 2012; 11(5):2721–2738. [PubMed: 22416763]

24. Donovan LE, Higginbotham L, Dammer EB, Gearing M, Rees HD, Xia Q, Duong DM, Seyfried NT, Lah JJ, Levey AI. Analysis of a membrane-enriched proteome from postmortem human brain tissue in Alzheimer's disease. PROTEOMICS – Clinical Applications. 2012; 6(3–4):201–211. [PubMed: 22532456]

25. Gozal YM, Duong DM, Gearing M, Cheng D, Hanfelt JJ, Funderburk C, Peng J, Lah JJ, Levey AI. Proteomics Analysis Reveals Novel Components in the Detergent-Insoluble Subproteome in Alzheimer's Disease. Journal of Proteome Research. 2009; 8(11):5069–5079. [PubMed: 19746990]

26. Silva JC, Gorenstein MV, Li G-Z, Vissers JPC, Geromanos SJ. Absolute Quantification of Proteins by LCMSE : A Virtue of Parallel ms Acquisition. Molecular & Cellular Proteomics. 2006; 5(1): 144–156. [PubMed: 16219938]

27. Schiess R, Mueller LN, Schmidt A, Mueller M, Wollscheid B, Aebersold R. Analysis of Cell Surface Proteome Changes via Label-free, Quantitative Mass Spectrometry. Molecular & Cellular Proteomics. 2009; 8(4):624–638. [PubMed: 19036722]

28. Huang DW, Sherman BT, Lempicki RA. Systematic and integrative analysis of large gene lists using DAVID bioinformatics resources. Nat. Protocols. 2009; 4(1):44–57.

29. Reich M, Liefeld T, Gould J, Lerner J, Tamayo P, Mesirov JP. GenePattern 2.0. Nat Genet. 2006; 38(5):500–501. [PubMed: 16642009]

30. de Hoon MJL, Imoto S, Nolan J, Miyano S. Open source clustering software. Bioinformatics. 2004; 20(9):1453–1454. [PubMed: 14871861]

31. Cline MS, Smoot M, Cerami E, Kuchinsky A, Landys N, Workman C, Christmas R, Avila-Campilo I, Creech M, Gross B, Hanspers K, Isserlin R, Kelley R, Killcoyne S, Lotia S, Maere S, Morris J, Ono K, Pavlovic V, Pico AR, Vailaya A, Wang P-L, Adler A, Conklin BR, Hood L, Kuiper M, Sander C, Schmulevich I, Schwikowski B, Warner GJ, Ideker T, Bader GD. Integration of biological networks and gene expression data using Cytoscape. Nat. Protocols. 2007; 2(10): 2366–2382.

32. Jensen LJ, Kuhn M, Stark M, Chaffron S, Creevey C, Muller J, Doerks T, Julien P, Roth A, Simonovic M, Bork P, von Mering C. STRING 8—a global view on proteins and their functional interactions in 630 organisms. Nucleic Acids Research. 2009; 37(suppl 1):D412–D416. [PubMed: 18940858]

33. Szklarczyk D, Franceschini A, Kuhn M, Simonovic M, Roth A, Minguez P, Doerks T, Stark M, Muller J, Bork P, Jensen LJ, Mering Cv. The STRING database in 2011: functional interaction networks of proteins, globally integrated and scored. Nucleic Acids Research. 2011; 39(suppl 1):D561–D568. [PubMed: 21045058]

34. Seyfried NT, Gozal YM, Donovan LE, Herskowitz JH, Dammer EB, Xia Q, Ku L, Chang J, Duong DM, Rees HD, Cooper DS, Glass JD, Gearing M, Tansey MG, Lah JJ, Feng Y, Levey AI, Peng J. Quantitative analysis of the detergent-insoluble brain proteome in frontotemporal lobar degeneration using SILAC internal standards. J Proteome Res. 2012; 11(5):2721–2738. [PubMed: 22416763]

35. Hayashi Y, Nihonmatsu-Kikuchi N, Hisanaga S-i, Yu X-j, Tatebayashi Y. Neuropathological Similarities and Differences between Schizophrenia and Bipolar Disorder: A Flow Cytometric Postmortem Brain Study. PLoS ONE. 2012; 7(3):e33019. [PubMed: 22438888]

36. Vitbitskii VN, Marakueva IV. Postmortem Changes in the Ultrastructure, Cytoplasmic Proteins and Nuclear Chromatin of Rabbit Nerve Cells. Arkh Anat Gistol Embriol. 1980; 79(11):79–85. [PubMed: 7458699]

37. Gonzalez F, Delahodde A, Kodadek T, Johnston SA. Recruitment of a 19S Proteasome Subcomplex to an Activated Promoter. Science. 2002; 296(5567):548–550. [PubMed: 11964484]

38. Hadjiolov AA, Tencheva ZS, Bojadjieva-Mikhailova AG. Isolation and Some Characteristics of Cell Nuclei from Brain Cortex of Adult Cat. The Journal of Cell Biology. 1965; 26(2):383–393. [PubMed: 5325391]

39. Deal RB, Henikoff S. The INTACT method for cell type-specific gene expression and chromatin profiling in Arabidopsis thaliana. Nat. Protocols. 2011; 6(1):56–68.

40. Dredge BK, Jensen KB. NeuN/Rbfox3 Nuclear and Cytoplasmic Isoforms Differentially Regulate Alternative Splicing and Nonsense-Mediated Decay of Rbfox2. PLoS ONE. 2011; 6(6):e21585. [PubMed: 21747913]

41. Kim KK, Adelstein RS, Kawamoto S. Identification of Neuronal Nuclei (NeuN) as Fox-3, a New Member of the Fox-1 Gene Family of Splicing Factors. Journal of Biological Chemistry. 2009; 284(45):31052–31061. [PubMed: 19713214]

42. Sosa, Brian A.; Rothballer, A.; Kutay, U.; Schwartz, Thomas U. LINC Complexes Form by Binding of Three KASH Peptides to Domain Interfaces of Trimeric SUN Proteins. Cell. 2012; 149(5):1035–1047. [PubMed: 22632968]

43. Wang W, Shi Z, Jiao S, Chen C, Wang H, Liu G, Wang Q, Zhao Y, Greene MI, Zhou Z. Structural insights into SUN-KASH complexes across the nuclear envelope. Cell Res. 2012; 22(10):1440–1452. [PubMed: 22945352]

44. Lee D, Ezhkova E, Li B, Pattenden SG, Tansey WP, Workman JL. The Proteasome Regulatory Particle Alters the SAGA Coactivator to Enhance Its Interactions with Transcriptional Activators. Cell. 2005; 123(3):423–436. [PubMed: 16269334]

45. Malik S, Shukla A, Sen P, Bhaumik SR. The 19 S Proteasome Subcomplex Establishes a Specific Protein Interaction Network at the Promoter for Stimulated Transcriptional Initiation in Vivo. Journal of Biological Chemistry. 2009; 284(51):35714–35724. [PubMed: 19843524]

46. Uprety B, Lahudkar S, Malik S, Bhaumik SR. The 19S proteasome subcomplex promotes the targeting of NuA4 HAT to the promoters of ribosomal protein genes to facilitate the recruitment of TFIID for transcriptional initiation in vivo. Nucleic Acids Research. 2012; 40(5):1969–1983. [PubMed: 22086954]

47. Yudkovsky N, Ranish JA, Hahn S. A transcription reinitiation intermediate that is stabilized by activator. Nature. 2000; 408(6809):225–229. [PubMed: 11089979]

48. Berg, Michael G.; Singh, Larry N.; Younis, I.; Liu, Q.; Pinto, Anna M.; Kaida, D.; Zhang, Z.; Cho, S.; Sherrill-Mix, S.; Wan, L.; Dreyfuss, G. U1 snRNP Determines mRNA Length and Regulates Isoform Expression. Cell. 2012; 150(1):53–64. [PubMed: 22770214]

49. Kaida D, Berg MG, Younis I, Kasim M, Singh LN, Wan L, Dreyfuss G. U1 snRNP protects pre-mRNAs from premature cleavage and polyadenylation. Nature. 2010; 468(7324):664–668. [PubMed: 20881964]

50. Noegel AA, Neumann S. The Role of Nesprins as Multifunctional Organizers in the Nucleus and the Cytoskeleton. Biochem. Soc. Trans. 2011; 39(6):1725–1728. [PubMed: 22103515]

51. Steiner FA, Talbert PB, Kasinathan S, Deal RB, Henikoff S. Cell-type-specific nuclei purification from whole animals for genome-wide expression and chromatin profiling. Genome Research. 2012; 22(4):766–777. [PubMed: 22219512]

52. Watakabe A. Comparative molecular neuroanatomy of mammalian neocortex: What can gene expression tell us about areas and layers? Development, Growth & Differentiation. 2009; 51(3):343–354.

53. Ransohoff RM, Brown MA. Innate immunity in the central nervous system. The Journal of Clinical Investigation. 2012; 122(4):1164–1171. [PubMed: 22466658]

54. Ghosh S, May MJ, Kopp EB. NF-κB AND REL PROTEINS: Evolutionarily Conserved Mediators of Immune Responses. Annual Review of Immunology. 1998; 16(1):225–260.

55. Lin, S.; Garcia, BA. Chapter One - Examining Histone Posttranslational Modification Patterns by High-Resolution Mass Spectrometry. In: Carl, W.; Allis, CD., editors. Methods in Enzymology. Vol. Vol. Volume 512. Academic Press; 2012. p. 3-28.

56. Zhang K, Schrag M, Crofton A, Trivedi R, Vinters H, Kirsch W. Targeted proteomics for quantification of histone acetylation in Alzheimer's disease. PROTEOMICS. 2012; 12(8):1261–1268. [PubMed: 22577027]
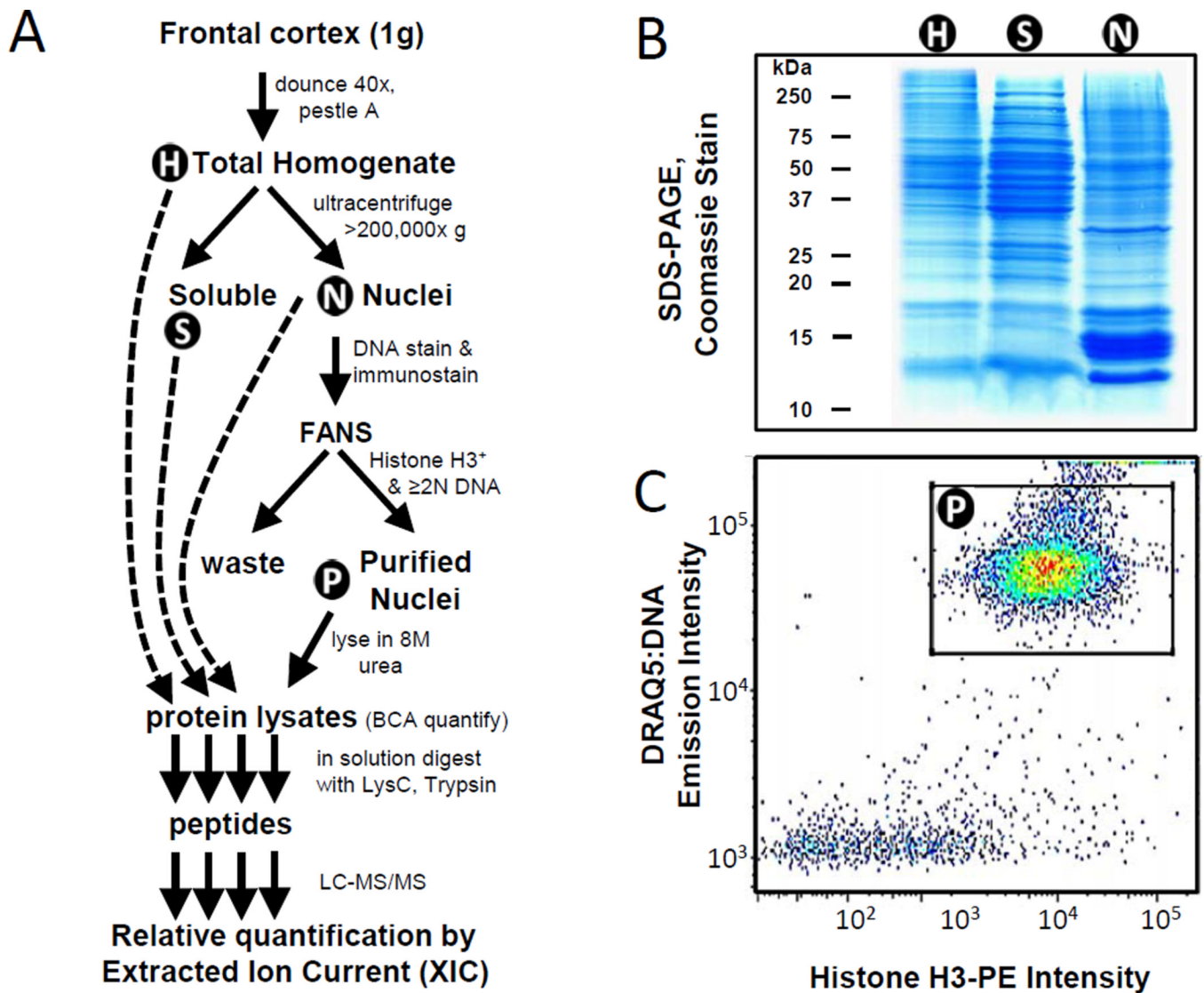
Figure 1. Workflow for the isolation and purification of nuclei from brain by FANS
(**A**) Workflow beginning human postmortem frontal cortex tissue (~1 g), through centrifugation, FANS, LC-MS/MS, and quantification yields four protein-rich fractions: total homogenate (**H**), soluble (**S**), nuclei obtained following ultracentrifugation (**N**), and FANS purified nuclei (**P**). (**B**) Total homogenate (**H**), soluble (**S**), nuclei (**N**) protein extracts visualized by Coomassie Blue G-250 stain in a 12% SDS-PAGE gel. (**C**) The FANS sorted nuclei are positive for DNA (DRAQ5®) and histone H3.
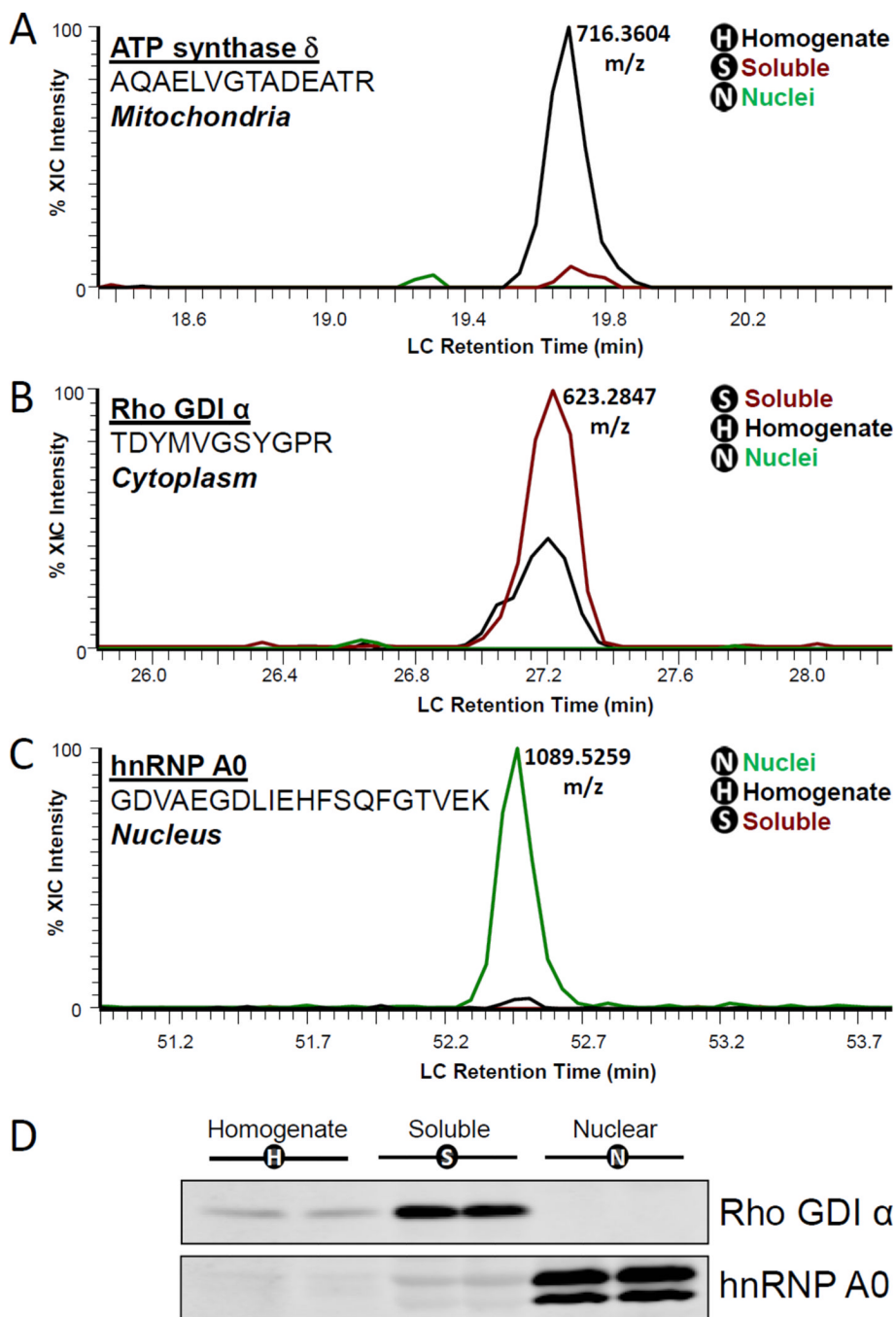
Figure 2. Purification strategy enriches for nuclear targets
(**A**) Overlay of the tryptic peptide precursor extracted ion chromatograms (XICs) for mitochondrial marker ATP synthase subunit delta (AQAELVGTADEATR) across Total homogenate (**H**), soluble (**S**), nuclei (**N**) fractions prior to FANS. (**B**) Overlay of the tryptic peptide precursor XICs for cytoplasmic marker Rho GDI alpha (TDYMVGSYGPR) across **H, S**, and **N** fractions. (**C**) Overlay of tryptic peptide precursor XICs for nuclear marker hnRNP A0 (GDVAEGDLIEHFSQFGTVEK) across **H, S**, and **N** fractions. (**D**) Western blots of Rho GDI alpha and hnRNP A0 in two biological replicates across **H, S**, and **N** fractions.
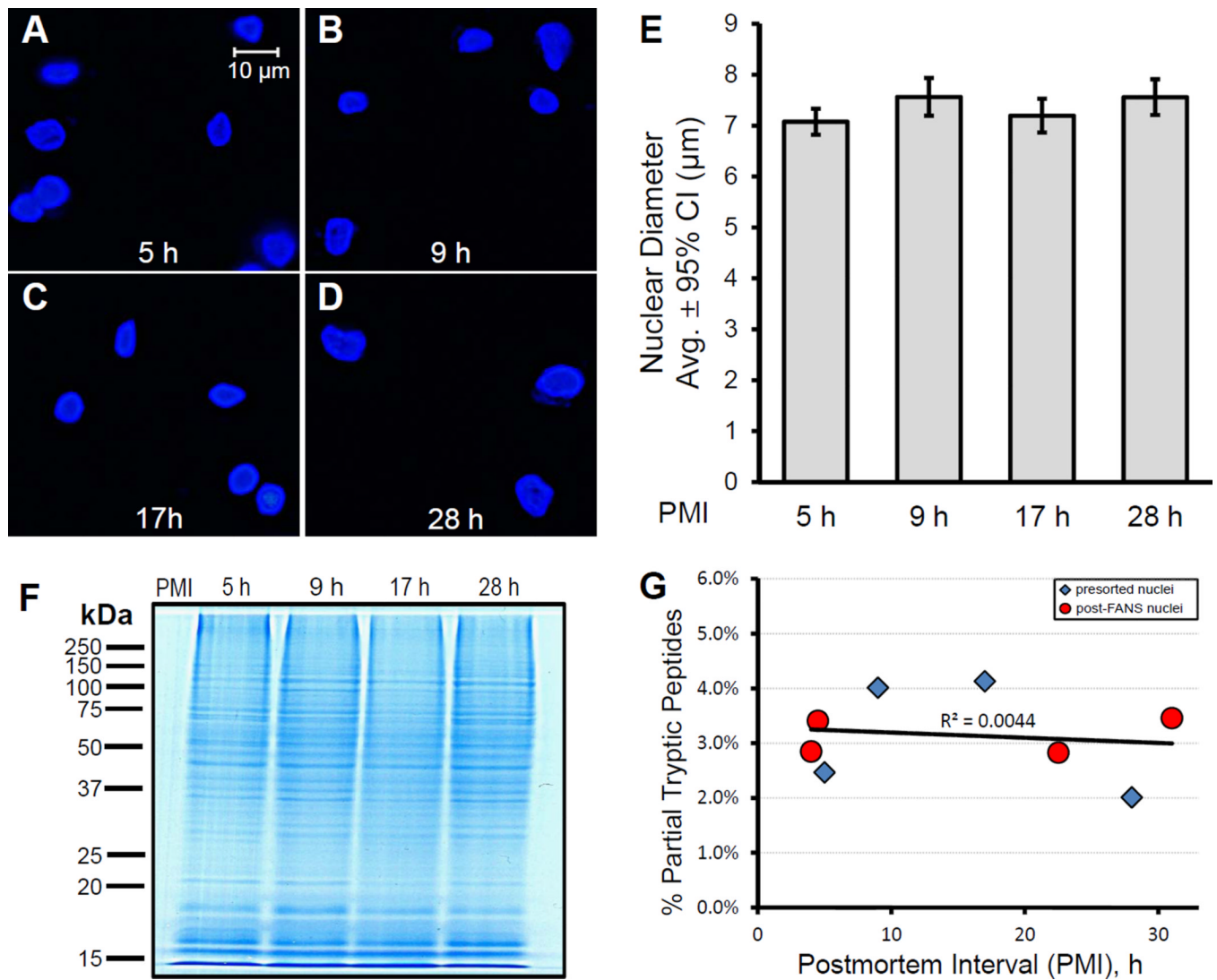
Figure 3. Nuclei isolated from frontal cortex retain structural and proteomic integrity even with extended post-mortem interval

(**A–D**) Fluorescent images of Hoechst-stained nuclei from individual cases with PMI varying from 5 h to 28 h as indicated. Scale bar, 10 μm. (**E**) Nuclear diameter average of 45 nuclei for each individual case represented by images in (**A–D**) was determined ± the 95 percent confidence interval. (**F**) Lysed nuclei protein extracts (25 μg) in 8M urea were resolved by electrophoresis on a 10% SDS-PAGE gel and visualized by Coomassie blue G250 staining. (**G**) The percentage of partial tryptic peptide identifications from LC-MS/MS was determined for 8 nuclear samples pre- and post-FANS.
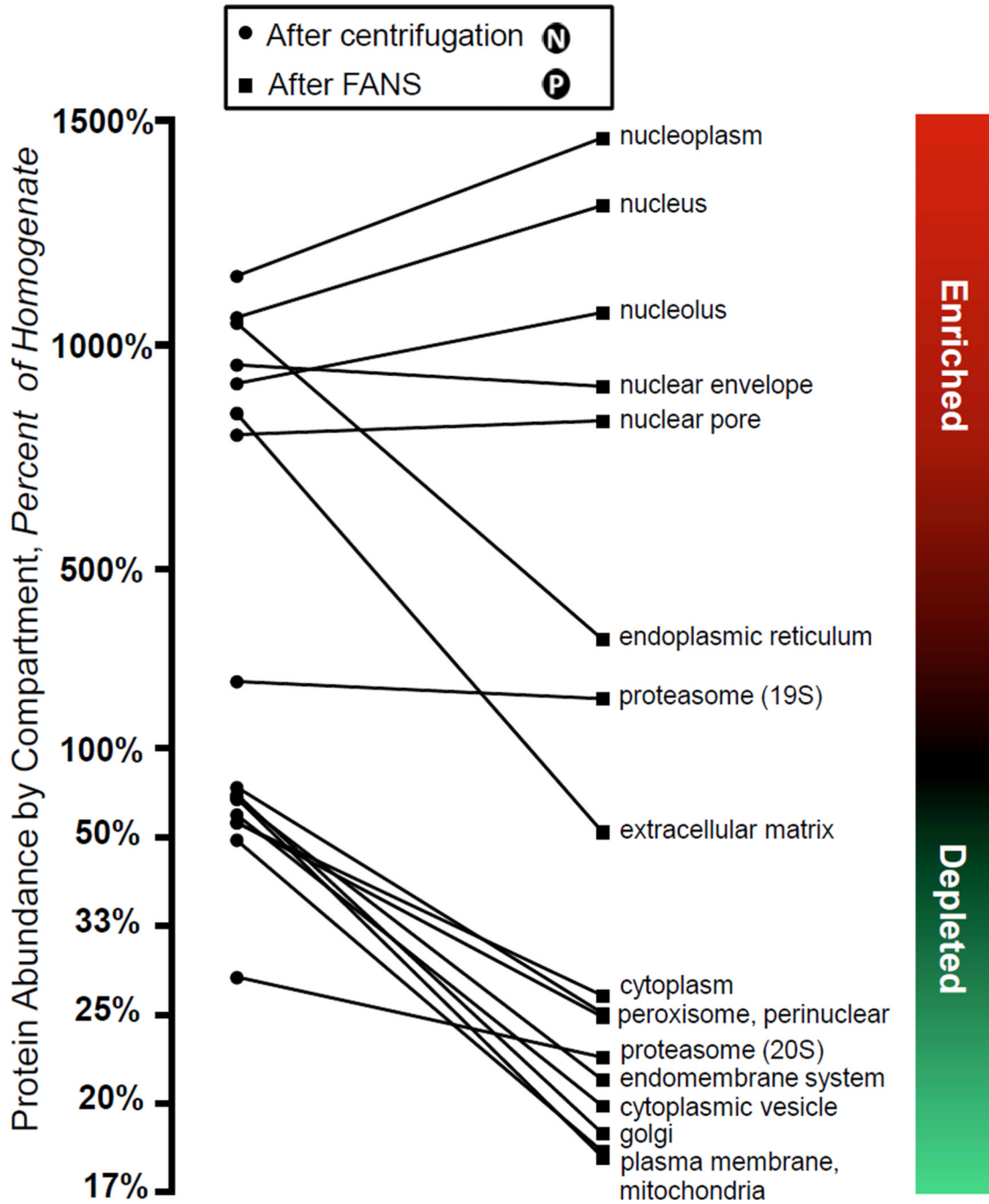
Figure 4. FANS reduces non-nuclear protein contamination
Protein groups were identified by DAVID ontology analysis of proteins determined to be enriched or depleted in pair-wise comparisons of i) pre-FANS nuclei (**N**) versus total homogenate (**H**) or ii) FACS-purified nuclei (**P**) versus total homogenate (**H**). The relative enrichment or depletion of each protein group scored as an aggregate protein ratio as described in experimental procedures and is indicated by a circle for **N/H** or a square for **P/H** ratios and indicate a trend towards enrichment or depletion, respectively.
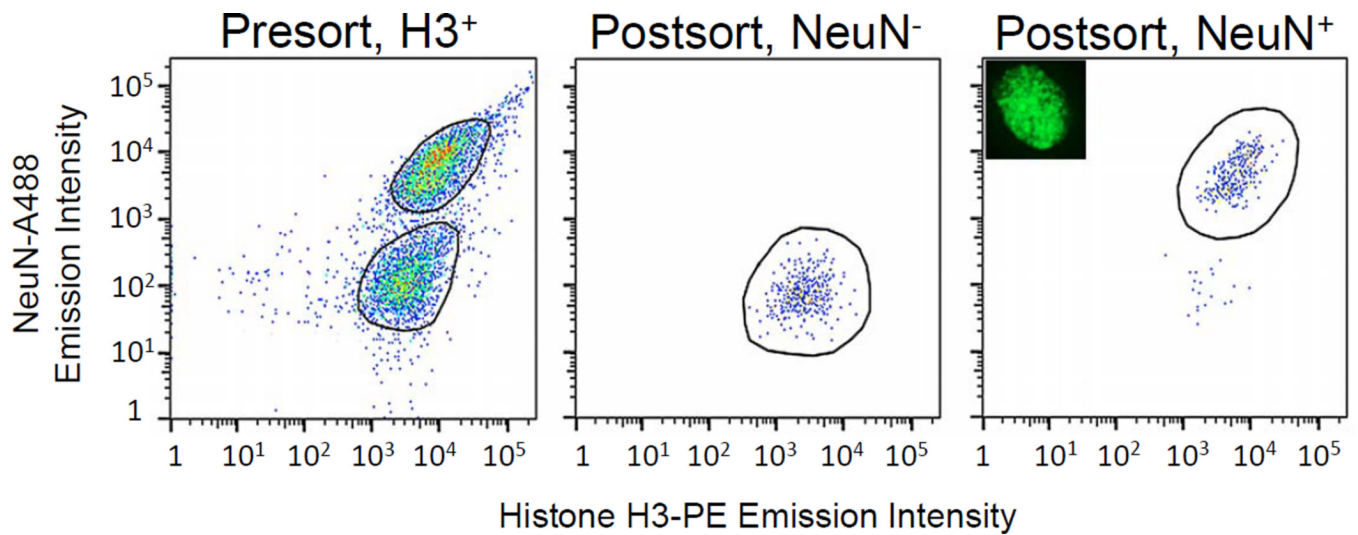
Figure 5. Isolation of neuronal and non-neuronal nuclei from human post-mortem brain tissue
Over five million nuclei were stained with DNA stain DRAQ5®, as well as NeuN and histone H3 fluorescent antibody conjugates and sorted by FANS into DNA positive, histone H3 positive subpopulations on a BD Biosciences FACSAria (*left panel*). The NeuN negative and positive populations were then resorted for 10,000 events to confirm purity after the initial sort (*middle and right panels*) Inset at the top left of the right panel is a representative picture of NeuN-Alexa Fluor® 488 stained nuclei recovered after FANS.
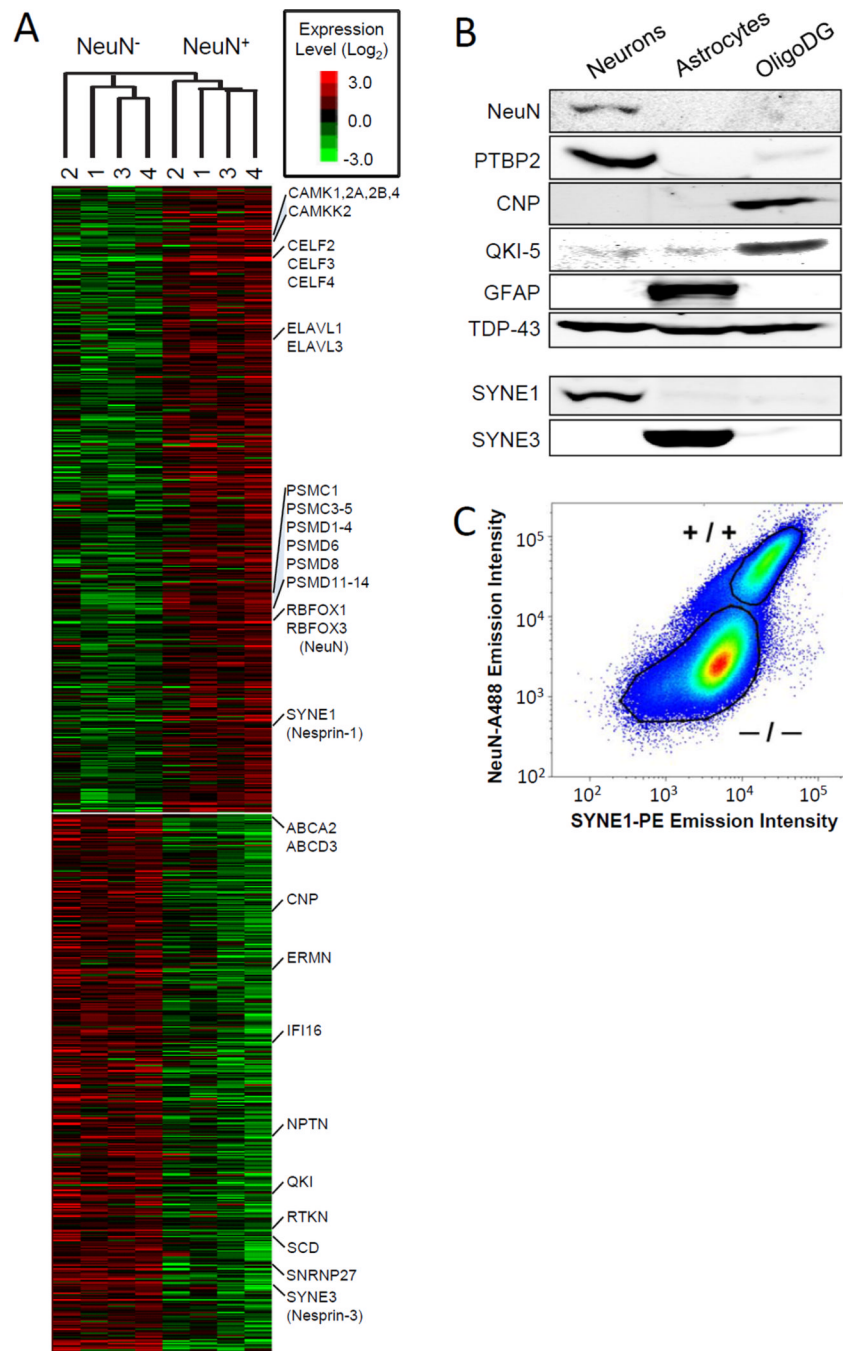
Figure 6. Clustering of FANS-separated nuclear proteomes defines neuronal and glial enriched proteins

(**A**) A dendrogram was produced by hierarchical clustering, correctly segregating NeuN negative and positive sorted samples. The top two groups of individual proteins, rows, found by k-means clustering are shown. Top and bottom clusters are 487 NeuN positive and 420 NeuN negative enriched nuclear proteins, respectively. Selected rows are identified to the right by gene symbol. (**B**) Western blot analysis of total homogenates from primary cultured rat neurons, astrocytes and oligodendrocytes (OligoDG) confirm specificity of RBFOX3 (NeuN) and PTBP2 expression in neurons. Conversely, known oligodendrocyte markers QKI (isoform 5) and CNP co-segregated with other proteins enriched in the NeuN negative

nuclear proteome. The nesprin paralogs nesprin-1 (SYNE1) and nesprin-3 (SYNE3) were observed specifically in neurons and astrocytes, respectively, consistent with proteomic results for isolated nuclei. TDP-43 was blotted as a loading control. (**C**) Flow cytometry for more than one million events pre-gated for DRAQ5® positive signal indicates separation of a NeuN and nesprin-1 positive population from a NeuN negative population with lower (background) levels of nesprin-1 staining intensity.

Table 1

Proteins significantly enriched in neuronal nuclei

Gene Symbol	RefSeq ID	RefSeq ID	Total Peptides	% Coverage	p value	Fold* Change NeuN+/NeuN-	Total Spectral Counts NeuN Negative				NeuN Positive			
							Case 1	Case 2	Case 3	Case 4	Case 1	Case 2	Case 3	Case 4
RNA Binding/Processing														
RBFOX3	**NP_001076044.1**	**RNA binding protein fox-1 homolog 3 (NeuN)**	**10**	**35%**	**1.31E-02**	**22.3**	**0**	**0**	**0**	**0**	**13**	**7**	**8**	**17**
CELF2	NP_001020248.1	CUGBP Elav-like family member 2	15	28%	1.54E-02	19.5	0	1	0	1	13	9	8	17
CELF	NP_011166120.1	CUGBP Elav-like family member 3	4	11%	9.15E-03	19.3	0	0	0	0	3	2	2	5
RBFOX1	NP_665899.1	RNA binding protein fox-1 homolog 1	11	38%	1.68E-02	16.5	0	0	0	0	14	5	8	17
ADARB1	NP_056648.1	double-stranded RNA-specific editase 1	15	32%	7.02E-04	11.5	0	0	0	0	8	11	13	9
WBP11	NP_057396.1	WW domain-binding protein 11	7	12%	1.27E-02	4.7	0	1	0	2	6	2	9	1
HNRNPD	NP_002129.2	heterogeneous nuclear ribonucleoprotein D0	23	59%	7.97E-04	4.3	3	12	7	11	24	32	28	44
SMU1	NP_060695.2	WD40 repeat-containing protein SMU1	13	32%	2.95E-02	3.6	2	8	0	3	11	8	6	10
HNRNPA0	NP_006796.1	heterogeneous nuclear ribonucleoprotein A0	17	56%	8.64E-03	3.4	6	9	10	9	19	15	18	22
CPSF2	NP_059133.1	cleavage and polyadenylation specificity factor subunit 2	6	13%	2.87E-02	3.3	0	3	0	0	1	3	4	0
HNRNPH1	NP_005511.1	heterogeneous nuclear ribonucleoprotein H	21	57%	1.64E-03	2.8	11	27	14	18	37	38	32	39
RBM2	NP_002130.2	heterogeneous nuclear ribonucleoprotein G	30	58%	2.28E-02	2.8	11	11	8	13	36	26	24	32
NOVA2	NP_002507.1	RNA-binding protein Nova-2	16	43%	1.73E-02	2.4	0	4	0	1	19	15	15	22
CPSF6	NP_008938.2	cleavage and polyadenylation specificity factor subunit 6	6	16%	4.50E-02	2.1	0	3	1	1	2	6	3	5
PARN	NP_001229921.1	poly(A)-specific ribonuclease PARN	7	13%	4.65E-02	1.9	0	0	0	0	4	1	3	5
Transcription factor or co-regulator														
ZNF483	NP_001007170.1	zinc finger protein 483	3	13%	2.76E-04	20.0	0	0	0	0	3	3	2	3
MLLT11	NP_006809.1	protein AF1q	5	73%	8.79E-03	17.4	0	0	0	0	1	2	3	6
ERH	NP_004441.1	enhancer of rudimentary homolog	3	18%	1.24E-02	10.5	1	1	0	0	3	1	2	2
SATB1	NP_002962.1	DNA-binding protein SATB1	7	12%	1.66E-03	10.3	0	0	0	0	3	3	8	5

Gene Symbol	RefSeq ID	RefSeq ID	Total Peptides	% Coverage	p value	Fold* Change $\frac{NeuN^+}{NeuN^-}$	Total Spectral Counts — NeuN Negative				Total Spectral Counts — NeuN Positive			
							Case 1	Case 2	Case 3	Case 4	Case 1	Case 2	Case 3	Case 4
TBR1	NP_006584.1	T-box brain protein 1	9	22%	7.54E-04	9.0	0	0	0	0	5	4	9	9
PNMA1	NP_006020.4	paraneoplastic antigen Ma1	8	29%	1.36E-02	8.5	0	0	0	0	6	1	1	8
DPF1	NP_004638.2	zinc finger protein neuro-d4	4	14%	1.44E-03	8.4	0	0	0	0	0	3	3	3
MYT1	NP_055840.2	myelin transcription factor 1-like protein	4	4%	1.05E-04	8.1	0	0	0	0	0	0	5	3
CRTC1	NP_056136.2	CREB-regulated transcription coactivator 1	2	4%	1.43E-02	7.8	0	0	0	0	3	0	2	3
PHYHIP	NP_001092805.1	phytanoyl-CoA hydroxylase-interacting protein	8	24%	6.19E-05	6.8	0	0	0	1	9	7	13	14
NCOA5	NP_066018.1	nuclear receptor coactivator 5	9	20%	2.50E-03	6.5	0	1	0	0	6	6	2	7
NCOR1	NP_006302.2	nuclear receptor corepressor 1	8	5%	1.20E-02	6.4	0	1	0	0	3	1	6	5
PSMD11	NP_002806.2	26S proteasome non-ATPase regulatory subunit 11	18	52%	6.91E-03	5.6	0	3	1	2	5	17	11	16
PSMC5	NP_002796.4	26S protease regulatory subunit 8	12	43%	5.66E-04	4.3	0	5	0	1	8	10	10	13
SMARCA1	NP_001007469.1	SWI/SNF-related matrix-associated actin-dependent regulator of chromatin B1	4	16%	2.81E-02	4.2	0	2	0	0	0	2	1	2
ARNT2	NP_055677.3	aryl hydrocarbon receptor nuclear translocator 2	10	27%	1.40E-03	3.5	0	0	0	0	4	6	10	11
PSMC3	NP_002795.2	26S protease regulatory subunit 6A	15	41%	9.09E-03	2.9	0	9	7	6	17	26	22	26
BTAF1	NP_003963.1	TATA-binding protein-associated factor 172	16	12%	2.46E-02	2.8	0	2	0	2	11	3	11	9
PURB	NP_150093.1	transcriptional activator protein Pur-beta	5	23%	3.59E-02	2.4	0	0	0	0	3	3	5	3
GTF2H1	NP_001135779.1	general transcription factor IIH subunit 1	2	4%	3.51E-02	2.2	0	0	0	0	1	0	4	1
Protein Kinase														
MAPK10	NP_002744.1	mitogen-activated protein kinase 10	5	14%	2.57E-04	11.8	0	0	0	0	0	5	2	4
PRKCG	NP_002730.1	protein kinase C gamma type	7	10%	4.03E-03	10.1	0	0	0	0	3	6	3	4
CAMK4	NP_001735.1	calcium/calmodulin-dependent protein kinase type IV	15	37%	1.30E-02	8.1	0	0	0	0	11	1	11	14
CAMKK2	NP_705720.1	calcium/calmodulin-dependent protein kinase kinase 2	5	14%	1.13E-02	4.7	0	0	0	0	6	1	5	4
CDK5	NP_004926.1	cyclin-dependent kinase 5	9	41%	8.42E-04	4.7	0	0	0	2	5	8	7	8

Gene Symbol	RefSeq ID	RefSeq ID	Total Peptides	% Coverage	p value	Fold* Change $\frac{NeuN^+}{NeuN^-}$	Total Spectral Counts							
							NeuN Negative				NeuN Positive			
							Case 1	Case 2	Case 3	Case 4	Case 1	Case 2	Case 3	Case 4
CAMK2B	NP_742081.1	calcium/calmodulin-dependent protein kinase type II subunit beta	19	39%	4.64E-04	3.8	11	10	11	12	24	25	30	22
CAMK2A	NP_741960.1	calcium/calmodulin-dependent protein kinase type II subunit alpha	24	50%	1.25E-04	3.4	15	14	20	19	46	34	43	33
Endoplasmic Reticulum/Structural														
ENC1	NP_003624.1	ectoderm-neural cortex protein 1	5	10%	2.28E-02	11.8	0	0	0	0	0	0	5	5
SYNE1	NP_892006.3	nesprin-1	37	6%	3.16E-02	1.9	0	1	0	0	17	4	28	12

NeuN (bold) monoclonal antibody was used to sort neuronal nuclei from frontal cortex.

*Fold change was determined by extracted ion intensity (relative abundance).